

2018

XUV-assisted high-order-harmonic-generation spectroscopy

T. S. Sarantseva

Voronezh State University, sartan86@mail.ru

M. V. Frolov

Voronezh State University, Russia, frolov@phys.vsu.ru

N. L. Manakov

Voronezh State University, manakov@phys.vsu.ru

A. A. Silaev

Institute of Applied Physics, Russian Academy of Sciences

N. V. Vvedenskii

Institute of Applied Physics, Russian Academy of Sciences

See next page for additional authors

Follow this and additional works at: <http://digitalcommons.unl.edu/physicsstarace>

 Part of the [Atomic, Molecular and Optical Physics Commons](#), [Elementary Particles and Fields and String Theory Commons](#), and the [Plasma and Beam Physics Commons](#)

Sarantseva, T. S.; Frolov, M. V.; Manakov, N. L.; Silaev, A. A.; Vvedenskii, N. V.; and Starace, Anthony F., "XUV-assisted high-order-harmonic-generation spectroscopy" (2018). *Anthony F. Starace Publications*. 233.
<http://digitalcommons.unl.edu/physicsstarace/233>

This Article is brought to you for free and open access by the Research Papers in Physics and Astronomy at DigitalCommons@University of Nebraska - Lincoln. It has been accepted for inclusion in Anthony F. Starace Publications by an authorized administrator of DigitalCommons@University of Nebraska - Lincoln.

Authors

T. S. Sarantseva, M. V. Frolov, N. L. Manakov, A. A. Silaev, N. V. Vvedenskii, and Anthony F. Starace

XUV-assisted high-order-harmonic-generation spectroscopyT. S. Sarantseva,^{1,2} M. V. Frolov,¹ N. L. Manakov,¹ A. A. Silaev,^{1,2,3} N. V. Vvedenskii,^{1,2,3} and Anthony F. Starace⁴¹*Department of Physics, Voronezh State University, Voronezh 394018, Russia*²*Institute of Applied Physics, Russian Academy of Sciences, Nizhny Novgorod 603950, Russia*³*Department of Radiophysics, University of Nizhny Novgorod, Nizhny Novgorod 603950, Russia*⁴*Department of Physics and Astronomy, University of Nebraska, Lincoln, Nebraska 68588-0299, USA*

(Received 29 October 2018; published 28 December 2018)

Using the analytic time-dependent effective range theory, we study two-color high-order harmonic generation (HHG) involving a weak extreme ultraviolet (XUV) pulse and an intense infrared laser field. Our analysis shows that XUV-assisted HHG spectra contain multiple additional plateau structures originating from absorption of one or more XUV photons at the photorecombination step of HHG. We show also that the HHG rate corresponding to the n th plateau can be presented in a factorized form involving the XUV-assisted (multiphoton) photorecombination cross section (PRCS) corresponding to absorption of n XUV photons of energy Ω and emission of a harmonic of energy Ω_h . This factorization allows one to extract the PRCS from the HHG spectrum and to retrieve the cross section of the inverse process: the photoionization cross section involving absorption of a single photon of energy Ω_h and emission of n XUV photons of frequency Ω . The analytic HHG results are in excellent agreement with numerical solutions of the three-dimensional time-dependent Schrödinger equation.

DOI: [10.1103/PhysRevA.98.063433](https://doi.org/10.1103/PhysRevA.98.063433)**I. INTRODUCTION**

High-order harmonic generation (HHG), produced by atoms or molecules in a strong infrared (IR) laser field, has attracted unflagging attention over the past few decades owing to the potential widespread impact of its many practical applications, including, e.g., the generation of coherent soft x-ray radiation [1–3], the production of attosecond pulses [4–6], and the detection and monitoring of ultrafast phenomena [7,8] (such as, e.g., light-induced electron tunnelling [5,6,9] or nuclear motion [10]). The rapidly developing area of HHG-based spectroscopy [11–13] provides a unique way of observing the electronic structure of atoms and molecules. It allows one to obtain single-photon photoionization cross sections (PICS) [12–19] and to image molecular orbitals [11,20–22]. The latter applications are based on the factorization of HHG rates in terms of a target-independent electron wave packet (EWP) and a single-photon photorecombination cross section (PRCS) [14–16,23] that is related to the PICS by the principle of detailed balance [24–26]. This factorization is based on the well-established three-step scenario of HHG in an IR field involving ionization, electron propagation in the laser field, and recombination of the laser-accelerated electron to the initial bound state of the target with emission of a high-energy photon [27].

The range of HHG applications may be extended by using a perturbative high-frequency XUV pulse in combination with a strong IR field. In experiments, the sources of the external XUV field are either a harmonic generated by the IR pulse itself [28–30] or the field of a synchronized free-electron laser (FEL) [31]. The presence of an additional XUV field significantly increases the number of possible channels in the HHG process and leads to novel structures in the HHG spectrum. Enhancement of the harmonic yield due to XUV-induced

resonancelike population of excited states of the target was investigated in Refs. [32–35]. Studies of XUV-enhanced HHG on the single-atom level have been carried out for either an attosecond pulse train [36–39] or an isolated attosecond pulse [40,41]. These studies have shown that the XUV pulse or pulses can be employed to control the ionization step and to select a specific electron trajectory contributing to the HHG yield. The addition of a weak XUV field was shown in Refs. [42,43] to result in extensions of the usual IR-field-induced HHG plateau. These plateau extensions were found to be one-electron phenomena and were attributed to XUV-field-induced ac-Stark modulations of the ground state and the returning EWP as recombination occurs [43]. Studies have also been carried out concerning the effects of XUV field population of resonant excited states from the valence shell of an atom, such as, e.g., Rabi oscillations [44–46].

If the energy of the XUV photon is large enough, inner-shell electrons may become involved in the HHG process, leading to an increase of the HHG plateau cutoff energy owing to the larger binding energy of core electrons [47–49]. The addition of an XUV field also leads to an extension of HHG spectroscopy methods that enable one to obtain information about inner-electron dynamics. Such extensions have been carried out to study Auger processes [50,51] and effects of resonant XUV-induced core-valence shell transitions [52].

Most studies cited above are focused on the HHG channel involving absorption of an XUV photon during the initial (ionization) step of the three-step HHG scenario. However, even in the single-active-electron approximation, there exist other channels for XUV-assisted HHG that remain so far insufficiently explored. Some of these additional channels may be ignored. Indeed, if the XUV photon is emitted at the ionization step, it effectively increases the ionization energy of an intermediate (virtual) state of the target thereby suppressing IR

tunneling from this virtual state [53]. Clearly that reduces the contribution of this channel to the HHG process. If interaction with the XUV field happens during the propagation step, then it induces multiple rescattering of the active electron, which, although important for low-energy harmonics, is negligible for the high-energy part of the harmonic spectrum [54,55]. Finally, the interaction with an XUV photon may be taken into account during the recombination step of HHG. In this case, emission of an XUV photon leads to a shortening of the high-energy plateau and hence the contribution of this channel is always masked by the contribution of the direct (XUV-free) IR channel. However, absorption of an XUV photon during the recombination step leads to an extension of the HHG plateau [55].

In this paper, we focus on XUV-assisted HHG processes involving this latter channel. When an XUV pulse of frequency Ω is added to a strong IR field, multiplet structures are formed in the HHG spectrum [42,43]. We show that the n th additional plateau is associated with the absorption of n XUV photons at the recombination step. We also show that the harmonic rate on the n th plateau is proportional to the PRCS with simultaneous absorption of n XUV photons of frequency Ω and emission of a single photon having the higher frequency $\Omega_h = n\Omega + E_n + I_p$, where E_n is the returning electron's kinetic energy and I_p is the ionization potential of the atom from which the active electron originated. [Atomic units (a.u.) are used throughout this paper, unless specified otherwise.] Finally, we show that the HHG rate in this channel can be presented in a factorized form involving the XUV-free EWP and the XUV-assisted (multiphoton) PRCS. This factorization allows one to extract the corresponding PRCS from the HHG spectrum and to find the cross section of the inverse process, i.e., the PICS involving absorption of a single photon of frequency Ω_h and emission of n XUV photons of frequency Ω .

This paper is organized as follows. In Sec. II we discuss time-dependent effective range (TDER) results for the HHG amplitude in a strong IR field and a weak XUV field. We also extend our model TDER results to the case of a neutral atomic system. In Sec. III we present a comparison of our analytic extended TDER-based results for XUV-assisted HHG with results obtained by numerical solution of the three-dimensional (3D) time-dependent Schrödinger equation (TDSE). We also present the procedure for retrieving multiphoton atomic PRCSs from the XUV-assisted HHG spectra. Our main results are summarized in Sec. IV and we discuss there the possibility of experimentally measuring the multiphoton PRCSs. Finally, in the Appendix we present a detailed derivation of the factorized result for the XUV-assisted HHG amplitude within the TDER approach, including the explicit form of the TDER result for the two-photon PRCS amplitude.

II. THEORETICAL ANALYSIS

A. TDER theory results for the XUV-assisted HHG amplitude

We consider the dipole interaction of an atomic system with linearly polarized IR and XUV fields,

$$\mathbf{F}(t) = \hat{\mathbf{z}}[F \cos(\omega t) + F_\Omega \cos(\Omega t)], \quad (1)$$

where F , ω , and F_Ω , $\Omega = k\omega$ (k is an integer, $k \gg 1$) are the field strengths and frequencies of the IR and XUV components, respectively. We assume the interaction of the atomic system with the IR field is realized in the tunneling regime (i.e., the Keldysh parameter $\gamma = \kappa\omega/F \ll 1$, $\kappa = \sqrt{2I_p}$), while the interaction with the XUV field may be treated in the perturbative regime ($\gamma_\Omega = \kappa\Omega/F_\Omega \gg 1$). In order to describe the interaction of an atom with a two-color field (1), we use the TDER approach [56,57]. General prescriptions for obtaining the analytical [beyond the strong-field approximation (SFA)] result for the HHG amplitude within the TDER approach have been presented in Ref. [23]. Here we omit calculations which are specific to the TDER theory (see the Appendix for details) and proceed directly to the general results. Since the XUV field is weak, we expand the exact HHG amplitude in a series in F_Ω , while keeping the nonperturbative contribution of the IR field.

The *zero order* in the XUV field result for the HHG amplitude has the well-known factorized form [14–16,23,58]

$$\mathcal{A}^{(0)}(\Omega_h) = a(E_0)f_{\text{rec}}^{(0)}(E_0), \quad E_0 = \Omega_h - I_p, \quad (2)$$

where E_0 is the returning electron's energy and Ω_h is the harmonic energy. The laser-induced factor $a(E_0)$, which describes the tunneling and propagation steps of the three-step scenario, has the form

$$a(E_0) = \frac{C_0}{\sqrt{2\pi i}} \frac{1}{T} \int_0^T dt \int_{-\infty}^t dt' \frac{e^{i(E_0+I_p)t - iS(t,t')}}{(t-t')^{3/2}}, \quad (3)$$

where $S(t, t')$ is the classical action for the active electron, which moves along a closed trajectory in the IR field with starting and ending times t' and t , respectively:

$$\begin{aligned} S(t, t') &= I_p(t - t') + \frac{1}{2} \int_{t'}^t P_0^2(\tau; t, t') d\tau, \\ \mathbf{P}_0(\tau; t, t') &= \frac{1}{c} \left[\mathbf{A}_0(\tau) - \frac{1}{t-t'} \int_{t'}^t \mathbf{A}_0(\tau') d\tau' \right], \\ \mathbf{A}_0(t) &= -\hat{\mathbf{z}}c \frac{F}{\omega} \sin(\omega t). \end{aligned} \quad (4)$$

The recombination amplitude, $f_{\text{rec}}^{(0)}(E_0)$, is the amplitude for a dipole transition from the continuum state $\psi_{\mathbf{k}_0}^{(+)}$ (satisfying outgoing wave asymptotic boundary conditions, with $\mathbf{k}_0 = k_0\hat{\mathbf{z}}$) to the bound state $\psi_0(\mathbf{r})$:

$$f_{\text{rec}}^{(0)}(E_0) = \langle \psi_0 | z | \psi_{\mathbf{k}_0}^{(+)} \rangle, \quad E_0 = k_0^2/2.$$

For the case of an atomic system with a single bound s state, we have

$$f_{\text{rec}}^{(0)}(E_0) = -i\sqrt{\pi\kappa}C_0 \frac{k_0^2}{\Omega_h^2}, \quad (5)$$

where C_0 is the dimensionless asymptotic coefficient of the field-free wave function in a short-range potential:

$$\psi_0(\mathbf{r})|_{\kappa r \gg 1} \rightarrow C_0 \sqrt{\frac{\kappa}{4\pi}} \frac{e^{-\kappa r}}{r}, \quad \kappa = \sqrt{2I_p}. \quad (6)$$

The HHG rate is given by the product of the EWP, $W(E_0)$, and the PRCS, $\sigma^{(0)}(E_0)$ [14–16,23,58],

$$R^{(0)}(\Omega_h) = \frac{\Omega_h^3}{2\pi c^3} |\mathcal{A}^{(0)}(\Omega_h)|^2 = W(E_0)\sigma^{(0)}(E_0), \quad (7)$$

where

$$W(E_0) = k_0 |a(E_0)|^2, \quad \sigma^{(0)}(E_0) = \frac{\Omega_h^3 |f_{\text{rec}}^{(0)}(E_0)|^2}{2\pi c^3 k_0}. \quad (8)$$

In the *first order* in F_Ω , the partial HHG amplitude with absorption of an XUV photon at the recombination step, $\mathcal{A}^{(1)}(\Omega_h)$, can be also presented in a factorized form (for details, see the Appendix):

$$\mathcal{A}^{(1)}(\Omega_h) = F_\Omega a(E_1) f_{\text{rec}}^{(1)}(E_1), \quad (9)$$

where $E_1 = \Omega_h - \Omega - I_p$ is the returning electron energy and $F_\Omega f_{\text{rec}}^{(1)}(E_1)$ is the amplitude for electron recombination (assisted by absorption of an XUV photon) with spontaneous emission of a photon having linear polarization along the z axis. The matrix element $f_{\text{rec}}^{(1)}(E_1)$ can be expressed in terms of the atomic Green function $G_{\mathcal{E}}$:

$$f_{\text{rec}}^{(1)}(E_1) = \langle \psi_0 | z G_{E_1 + \Omega z} | \psi_{\mathbf{k}_1}^{(+)} \rangle + \langle \psi_0 | z G_{E_1 - \Omega_h z} | \psi_{\mathbf{k}_1}^{(+)} \rangle, \quad (10)$$

where $E_1 = k_1^2/2$ and $\mathbf{k}_1 = k_1 \hat{\mathbf{z}}$. For the case of an initial s state $\psi_0(\mathbf{r})$, the dipole matrix element has the form [59]

$$f_{\text{rec}}^{(1)}(E_1) = -\frac{\sqrt{\pi} \kappa C_0}{2\Omega \Omega_h} \left\{ \frac{k_1^2}{\Omega \Omega_h} + \frac{1}{\Omega_h - \Omega} + \frac{1}{\mathcal{R}_0(E_1)} \left[\frac{\kappa + ik_1}{\Omega_h - \Omega} + \frac{\kappa^3 + ik_1^3 - ik_\Omega^3 - ik_{\Omega_h}^3}{3\Omega \Omega_h} \right] \right\}, \quad (11)$$

where

$$k_\Omega = \sqrt{2(E_1 + \Omega)}, \quad (12)$$

$$k_{\Omega_h} = \sqrt{2(E_1 - \Omega_h)},$$

and $\mathcal{R}_0(E)$ is defined by the s -wave scattering phase, $\delta_0(E)$:

$$\mathcal{R}_0(E) = \sqrt{2E} [\cot \delta_0(E) - i]. \quad (13)$$

We emphasize that the laser factor $a(E_1)$ has the same form as for the XUV-free case [see Eq. (3)], while, for the same harmonic energy Ω_h , the returning electron energy, E_1 , is shifted by the energy of the XUV photon from E_0 .

Although both amplitudes $\mathcal{A}^{(0)}(\Omega_h)$ and $\mathcal{A}^{(1)}(\Omega_h)$ contribute to the total HHG amplitude, their contributions are significant in two different energy ranges in Ω_h . Indeed, $\mathcal{A}^{(0)}(\Omega_h)$ contributes in the range $\Omega_h < \Omega_{\text{cut}}^{(0)} \approx 1.324I_p + 3.17u_p$ [where $u_p = F^2/(4\omega^2)$] in which plateau effects induced by the IR field are prominent; in this energy range $|\mathcal{A}^{(0)}(\Omega_h)| \gg |\mathcal{A}^{(1)}(\Omega_h)|$. For $\Omega_h > \Omega_{\text{cut}}^{(0)}$, the amplitude $\mathcal{A}^{(0)}(\Omega_h)$ rapidly decreases, while $\mathcal{A}^{(1)}(\Omega_h)$ oscillates with a smooth amplitude and gives the major contribution. Thus, for $\Omega_h > \Omega_{\text{cut}}^{(0)}$, the contribution from all other channels can be neglected and the HHG rate, $R \equiv R(\Omega_h)$, is given by the amplitude $\mathcal{A}^{(1)}(\Omega_h)$:

$$R \approx R^{(1)}(\Omega_h) = \frac{\Omega_h^3}{2\pi c^3} |\mathcal{A}^{(1)}(\Omega_h)|^2 = W(E_1) \sigma^{(1)}(E_1), \quad W(E_1) = k_1 |a(E_1)|^2, \quad (14)$$

where $\sigma^{(1)}$ is the XUV-assisted PRCS with absorption of a single XUV photon:

$$\sigma^{(1)}(E_1) = \frac{\Omega_h^3 F_\Omega^2}{2\pi c^3 k_1} |f_{\text{rec}}^{(1)}(E_1)|^2. \quad (15)$$

The EWP's $W(E_{0,1})$ in Eqs. (8) and (14) can be analytically estimated for those energies at which only one or two closed electron trajectories contribute significantly [16,58] (i.e., near the caustic energies [60–62]),

$$W(E) = \mathcal{I}(F, \omega) \mathcal{W}(E), \quad (16)$$

where the factors on the right side are defined as follows.

The *ionization factor*, $\mathcal{I}(F, \omega)$, is proportional to the detachment rate in the “effective” static electric field [63],

$$\mathcal{I}(F, \omega) = \frac{4\tilde{\gamma}^2}{\pi \kappa} \Gamma_{\text{st}}(\tilde{F}), \quad (17)$$

$$\Gamma_{\text{st}}(\tilde{F}) = I_p C_0^2 \frac{\tilde{F}}{2\kappa^3} e^{-\frac{2\kappa^3}{3\tilde{F}}}, \quad (18)$$

where $\tilde{F} \approx 0.95F$ is the instantaneous electric field (at the moment of ionization) and $\tilde{\gamma} = \omega\kappa/\tilde{F}$ is the corresponding effective Keldysh parameter.

The *propagation factor*, $\mathcal{W}(E_n)$, can be written in terms of the Airy function $\text{Ai}(\zeta)$:

$$\mathcal{W}(E_n) = \sqrt{2E_n} (\delta F^2)^{-2/3} \frac{\text{Ai}^2(\zeta)}{\Delta t^3}, \quad (19)$$

$$\zeta = \frac{E_n - E_{\text{max}}}{(\delta F^2)^{1/3}}, \quad n = 0, 1,$$

where $\Delta t \approx 0.65T$ is the electron travel time in the laser field, $E_{\text{max}} \approx 3.17u_p + 0.324I_p$ is the maximum energy gained, and $\delta = 0.536$.

B. Generalization of the TDER results to real atomic systems

Although our analytical TDER results are truly valid for the case of a short-range potential supporting only a single bound state [cf. Eq. (6)], they cannot be directly applied for the case of a neutral or positively charged system involving the long-range Coulomb interaction of the active (valence) electron with the core. However, based on a quasiclassical analysis [64], it was argued that in HHG the Coulomb field primarily affects the ionization step, enhancing it by a few orders of magnitude [65,66], while its effect on the electron's propagation in a strong laser field is only a slight perturbation. We thus introduce a Coulomb correction in accord with Ref. [64], which in fact consists in the replacement of the detachment rate in Eq. (16) by the corresponding atomic ionization rate:

$$W(E_n) \longrightarrow W_{\text{at}}(E_n) = \left(\frac{2\kappa^3}{\tilde{F}} \right)^{2\nu} W(E_n), \quad (20)$$

where $\nu = Z/\kappa$ is an effective quantum number and Z is the charge of the atomic core. The factorization proposed in Eqs. (7) and (14) requires also the replacement of the TDER XUV-assisted PRCS by the corresponding atomic counterpart: $\sigma^{(n)}(E_n) \rightarrow \sigma_{\text{at}}^{(n)}(E_n)$, $n = 0, 1$. As a result, we obtain

$$R^{(n)}(\Omega_h) = W_{\text{at}}(E_n) \sigma_{\text{at}}^{(n)}(E_n). \quad (21)$$

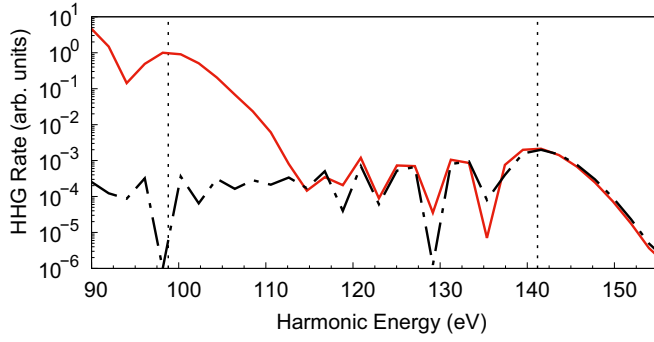


FIG. 1. Comparison of HHG rates for an atomic system with $I_p = 13.65$ eV in the two-color field (1) obtained using the analytic result in Eq. (14) (dot-dashed black line) with first order in XUV TDER model results [55] (solid red line). The parameters of the IR field are $\omega = 1$ eV ($\lambda = 1.2 \mu\text{m}$) and $I = 2 \times 10^{14}$ W/cm²; the intensity of the XUV field is the same as for the IR field and its frequency is $\Omega = 41$ eV. Vertical dotted lines mark HHG plateau cutoff positions. Left-hand dotted line: $\Omega_h = \Omega_{\text{cut}}^{(0)}$; right-hand dotted line: $\Omega_h = \Omega_{\text{cut}}^{(0)} + \Omega$.

III. RESULTS AND DISCUSSION

A. Numerical results

In order to check the accuracy of our analytical results, we first compare the HHG rate calculated using the analytic Eq. (14) with first order in XUV TDER results [55]. Calculations were done for an IR field with $\omega = 1$ eV ($\lambda = 1.2 \mu\text{m}$), intensity $I = 2 \times 10^{14}$ W/cm², and $\Omega = 41$ eV with $I_\Omega = I$, $C_0 = 2$, and $I_p = 13.65$ eV. The HHG spectra are presented in Fig. 1. It can be seen that even for equal intensities of the IR and XUV field components, for $\Omega_h < \Omega_{\text{cut}}^{(0)}$ the XUV-assisted HHG channel is four orders of magnitude less than the HHG rate produced by the IR field alone. However, in the energy region above the IR field cutoff ($\Omega > \Omega_{\text{cut}}^{(0)}$; marked in Fig. 1 by the left-hand vertical dotted line) the analytical result (14) for the HHG rate is found to be in excellent agreement with the TDER result [55] for energies ≥ 113 eV.

In Fig. 2(a) we compare our analytic results appropriate for a neutral system with numerical solutions of the 3D TDSE. The TDSE was solved by a split-step method using a fast Fourier transform for propagation along the z axis and a Hankel transformation for propagation in the transverse direction [67]. The hydrogen atom system in the TDSE calculations was modeled by using a soft-Coulomb potential:

$$U(r) = -\alpha \operatorname{sech}^2(r/a) - \tanh(r/a)/r, \quad (22)$$

with $\alpha = 0.3$, $a = 2.17$, which supports a $1s$ bound state having an ionization potential $I_p = 13.65$ eV. In our calculations the $1s$ state is the initial state. The laser pulse in our TDSE calculations for the field (1) was chosen to have a smoothed-trapezoidal envelope $f(t)$ comprised of a six-cycle flat top of constant intensity and a two-cycle \sin^2 ramp for turn on and turn off,

$$f(t) = \begin{cases} \sin^2(\pi t/4T), & 0 < t \leq 2T, \\ 1, & 2T < t \leq 8T, \\ \cos^2(\pi t/4T), & 8T < t \leq 10T, \\ 0, & t \leq 0, t > 10T, \end{cases} \quad (23)$$

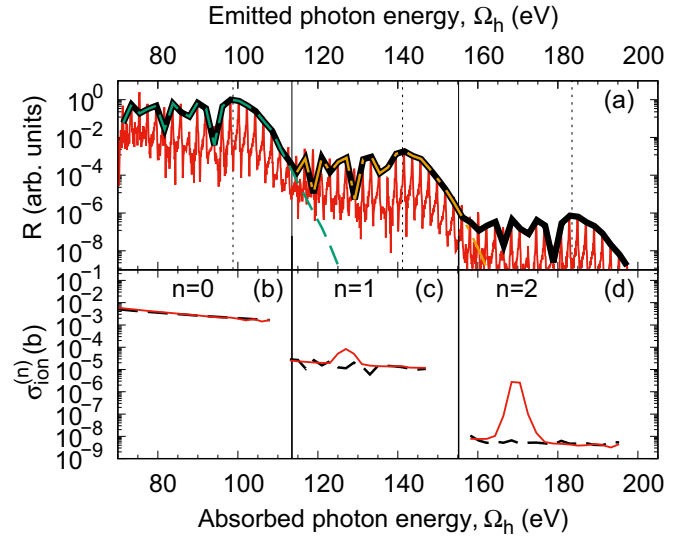


FIG. 2. Comparison of analytic and TDSE results for (a) XUV-assisted HHG spectra for a model system described by the potential (22) having an ionization potential ($I_p = 13.65$ eV) equal to that of the H atom and (b)–(d) corresponding multiphoton PICs, $\sigma_{\text{ion}}^{(n)}$, results (for absorption of an XUV photon of energy Ω_h and emission of n XUV photons of energy $\Omega = 41$ eV) in three energy regions of the HHG spectra. The laser field parameters are the same as in Fig. 1. The vertical dotted lines mark plateau cutoff positions according to Eq. (24), and the vertical solid thin lines mark the energy regions over which the HHG rates $R^{(n)}$ with $n = 0, 1, 2$ are dominant. Curves in (a): solid thin red line, TDSE results; solid thick black line, analytic result (25); dashed green line, analytic result (21) for $n = 0$; dot-dashed thick orange line, analytic result (21) for $n = 1$. Curves in (b)–(d): solid red lines, direct TDSE results (see text for details); dashed black lines show $\sigma_{\text{ion}}^{(n)}$ retrieved from the HHG spectrum in (a).

where $T = 2\pi/\omega$ is the period of the IR field. We obtain converged TDSE results for uniform grids of time and z coordinates with spacing $\Delta t = 0.02$ a.u., $\Delta z = 0.3$ a.u., and a total number of z -axis grid nodes $N_z = 2048$. In the perpendicular plane, for the polar coordinate (ρ) we used a nonuniform grid with $\rho_{\text{max}} = 74$ a.u. and a total number of nodes in the radial direction of $N_\rho = 480$. To avoid wave reflection effects, in our calculations we introduced absorption layers of width 30 a.u. [67].

It is seen from Fig. 2(a) that the XUV-assisted HHG spectrum exhibits multiple plateau structures separated by the XUV photon energy Ω with cutoffs near 99 eV, 141 eV, and 184 eV. The first plateau is produced by the IR field and its cutoff is found to agree with the expected value of $3.17u_p$. The second plateau results from the absorption of an XUV photon by an electron in the strong IR laser field and its cutoff is given by $\Omega^{(1)} = \Omega_{\text{cut}}^{(0)} + \Omega$. The shapes of both plateaus obtained by our TDSE calculations agree with the results of our analytic predictions in Eq. (21), where the cross sections, $\sigma_{\text{at}}^{(n)}$, were calculated numerically. Moreover, our highly precise TDSE calculations also show a third plateau, which we associate with absorption of two XUV photons in this XUV-assisted HHG process. This observation suggests an extension of Eq. (21) for any $n \geq 0$ with $E_n = E_0 - n\Omega$ and

$\sigma_{\text{at}}^{(n)} \propto F_{\Omega}^{2n}$, which is the n -XUV-photon-assisted PRCS in the lowest order in F_{Ω} .

Each rate $R^{(n)}(\Omega_h)$ contributes significantly only in the prescribed range of harmonic energies $\Omega_{\text{cut}}^{(n-1)} < \Omega_h < \Omega_{\text{cut}}^{(n)}$, where

$$\begin{aligned}\Omega_{\text{cut}}^{(n)} &= \Omega_{\text{cut}}^{(0)} + n\Omega, \quad \text{for } n = 0, 1, 2, \dots, \\ \Omega_{\text{cut}}^{(0)} &= 1.324I_p + 3.17u_p.\end{aligned}\quad (24)$$

Since each rate $R^{(n)}(\Omega_h)$ contributes mainly in a unique range of frequency Ω_h , we propose the following general expression for the ‘‘total’’ XUV-assisted HHG rate:

$$R(\Omega_h) = \sum_{n=0}^{\infty} R^{(n)}(\Omega_h). \quad (25)$$

B. Retrieval of multiphoton PICSs

The factorization (21) provides an extension of HHG-based spectroscopy that allows one to retrieve multiphoton PICS. Consider HHG peaks in XUV-assisted HHG spectra separated by the XUV photon energy Ω . According to Eq. (21), HHG rates for these peaks are determined by the same value of the EWP $W_{\text{at}}(E_n)$. Thus the ratio of any two rates is given by the ratio of the corresponding XUV-assisted PRCSs:

$$\frac{R^{(n+q)}(\Omega_h + q\Omega)}{R^{(n)}(\Omega_h)} = \frac{\sigma_{\text{at}}^{(n+q)}(E_{n+q})}{\sigma_{\text{at}}^{(n)}(E_n)}, \quad (26)$$

where n and q are positive integers. If the ‘‘reference’’ peak lies in the first (IR-field-induced) plateau, then we can express the XUV-assisted PRCS, $\sigma_{\text{at}}^{(n)}$, in terms of the field-free PRCS, $\sigma_{\text{at}}^{(0)}$ (which, for instance, can either be retrieved from XUV-free HHG spectra [12–15,17,18,21,22] or calculated numerically [68,69] using the principle of detailed balance [24–26]):

$$\sigma_{\text{at}}^{(n)}(E_n) = \frac{R^{(n)}(\Omega_h + n\Omega)}{R^{(0)}(\Omega_h)} \sigma_{\text{at}}^{(0)}(E_0). \quad (27)$$

The algorithm for obtaining an n -photon XUV-assisted PRCS for an arbitrary atom comprises three steps: (i) measuring the XUV-assisted HHG spectrum, (ii) calculating the ratio of HHG yields separated by the energy of n XUV photons, and (iii) multiplying this ratio by the XUV-free PRCS according to Eq. (27). The PRCS thus obtained is directly related to the PICS in the field of a two-color XUV pulse: the PRCS for the frequency Ω_h of the emitted photon and n absorbed Ω photons corresponds to the PICS for the inverse process, namely, the absorption of a single Ω_h photon and emission of n Ω photons.

Figures 2(b)–2(d) show PICSs corresponding to the emission of $n = 0, 1$, and 2 XUV photons with energy $\Omega = 41$ eV retrieved using Eq. (27) and the numerically calculated HHG spectrum shown in Fig. 2(a). As expected for the H atom, the PICSs are smooth, slowly decreasing functions of the absorbed XUV photon energy Ω_h . We compared retrieved PICSs with the TDSE results obtained from numerical solution of the TDSE for a long two-color linearly polarized XUV pulse with carrier frequencies Ω and Ω_h . In order to obtain the PICS from the TDSE results, we calculate the momentum distribution of the photoelectrons along the field polarization axis and select

those peaks corresponding to absorption of a single Ω_h photon and emission of several Ω photons.

As seen in Figs. 2(b)–2(d), the results of these calculations agree everywhere except in the neighborhoods of photoelectron energies $E = n\Omega - I_p$ for $n = 1, 2$. In these energy ranges, the direct TDSE method greatly overestimates the true value of the PICSs. This deviation originates from interference of the various possible pathways from a given initial state to the same final state. When an atom is ionized by a two-color field with an integer frequency ratio $m = \Omega_h/\Omega$, the energy of an electron that absorbs a photon of frequency Ω_h and emits n photons of frequency Ω exactly equals the energy of an electron that absorbs $m - n$ photons of frequency Ω . The probability of the second (absorption) process can be significantly larger than that of the first (absorption and emission) process. Consequently, the directly calculated TDSE PICS results contain peaks at photoelectron energies $E = (m - n)\Omega - I_p$, where $n \geq 1$, that do not exist in the PICSs retrieved from the XUV-assisted HHG spectra. These artifacts are clearly seen in Figs. 2(c) and 2(d), where the peaks corresponding to $m = 3, n = 1$ and $m = 4, n = 2$ overestimate the PICSs by one and three orders of magnitude, respectively. This pronounced overestimation is because the probability of absorption of two ‘‘soft’’ photons of frequency Ω significantly exceeds the probability of absorption of one photon of higher frequency $\Omega_h = 3\Omega$ or $\Omega_h = 4\Omega$ with subsequent emission of one or two photons of frequency Ω , respectively.

C. Measurement of multiphoton PICSs

Direct measurements of two-photon (or multiphoton) PICS in the XUV region confront a number of difficulties. At present, standard FEL-based two-color sources are well developed only for fixed frequencies close to harmonics of the seeding pulse [70,71], and, despite significant progress [70,71], frequency tuning over a wide energy range is still difficult. Another difficulty of direct multiphoton PICS measurements occurs if the frequency ratio of the XUV components is close to an integer. In this case, different multiphoton channels may result in the same final state of the ionized electron, thus leading to an interference between alternative transition amplitudes. Although this interference has stimulated a great interest recently concerning the coherent control of two- and three-photon ionization [72], it prevents measurements of the separate contributions of the interfering multiphoton channels. The XUV-assisted HHG spectroscopy method proposed in this paper avoids contributions from alternative ionization channels and thus opens up the unique possibility for extracting the partial cross sections of individual photoionization channels in two-color XUV ionization processes for a wide range of XUV frequencies.

IV. SUMMARY AND CONCLUSIONS

In summary, we have used TDER theory to investigate XUV-assisted HHG and have shown that the n th additional HHG plateau made possible by the XUV field (with photon energy Ω) originates from absorption of n XUV photons at the photorecombination step of HHG (where $n = 0$ is the usual HHG plateau produced by the IR field alone). We have also

shown that the HHG rate corresponding to the n th plateau can be presented in a factorized form involving the XUV-assisted (multiphoton) PRCS corresponding to absorption of n XUV photons of energy Ω and emission of a harmonic of energy Ω_h . This factorization allows one to extract the cross section of the inverse process (using the principle of detailed balance [24–26]), i.e., the PICS involving absorption of a single photon of energy Ω_h and emission of n XUV photons of frequency Ω .

We have also shown that a possible alternative method for finding n -XUV-photon-assisted PICSs, based on direct measurement of the photoelectron energy distribution in a two-color XUV field, fails to provide correct results for the case when the XUV frequency Ω_h is an integer multiple of the frequency Ω ($\Omega_h = m\Omega$) owing to the interference of different ionization channels having typically very different magnitudes. Our proposed HHG-based method of finding multiphoton PICS allows one to select a particular ionization channel and works for all values of the photoelectron energy. It also appears to offer a much simpler means for experimental realization.

ACKNOWLEDGMENTS

This work was supported in part by the Ministry of Science and Higher Education of the Russian Federation through Grant No. 3.1659.2017/4.6, the Russian Science Foundation through Grant No. 18-12-00476 (numerical calculations), by the Russian Foundation for Basic Research (Grant No. 16-32-60200), and by the U.S. National Science Foundation (NSF) through Grant No. PHY-1505492 (A.F.S.).

APPENDIX: TDER DERIVATION OF EQS. (16)–(19)

The HHG amplitude for the N th harmonic with frequency $\Omega_h = N\omega$ and polarization vector \mathbf{e}_h in a periodic field with period $T = 2\pi/\omega$ has the form

$$\mathcal{A}(\Omega_h) = \mathbf{e}_h^* \cdot \mathbf{d}(N),$$

where $\mathbf{d}(N)$ is the N th Fourier coefficient of the dual dipole moment of the quantum system [73]. One obtains $\mathbf{d}(N)$ from analysis of the complex quasienergy of the system in a two-component field described by the vector potential $\mathbf{A}'(t)$,

$$\mathbf{A}'(t) = \mathbf{A}(t) + \mathbf{A}_h(t), \quad (\text{A1})$$

where $\mathbf{A}(t)$ is the vector potential of the IR and XUV fields,

$$\mathbf{A}(t) = \mathbf{A}_0(t) + \mathbf{A}_1(t), \quad (\text{A2a})$$

$$\mathbf{A}_0(t) = -\mathbf{e}_z c \frac{F}{\omega} \sin(\omega t), \quad (\text{A2b})$$

$$\mathbf{A}_1(t) = -\mathbf{e}_z c \frac{F\Omega}{\Omega} \sin(\Omega t), \quad (\text{A2c})$$

and $\mathbf{A}_h(t)$ is the vector potential of the harmonic field with frequency Ω_h and polarization vector \mathbf{e}_h :

$$\mathbf{A}_h(t) = c \frac{F_h}{\Omega_h} \text{Im}[\mathbf{e}_h e^{-i\Omega_h t}]. \quad (\text{A3})$$

Here c is the speed of light and F_h is the amplitude of the probe harmonic field. The dipole moment $\mathbf{d}(N)$ can be presented as a derivative in $\mathbf{F}_h^* \equiv F_h \mathbf{e}_h^*$ of the first order in F_h quasienergy ϵ' in the two-component field (A1) [73]:

$$\mathbf{d}(N) = -2 \frac{\partial \epsilon'}{\partial \mathbf{F}_h^*} \Big|_{F_h=0}. \quad (\text{A4})$$

Within the TDER approach, the exact (without expansion in F_h) eigenvalue problem for the complex quasienergy ϵ' reduces to an infinite homogeneous system of linear equations for the Fourier coefficients f'_k of a periodic function $f'(t)$ [56,57]:

$$\sum_{k'} [\mathcal{R}_0(\epsilon' + 2k\omega) \delta_{k,k'} - M'_{k,k'}(\epsilon')] f'_k = 0, \quad (\text{A5})$$

$$M'_{k,k'}(\epsilon') = \frac{1}{\sqrt{2\pi i}} \frac{1}{T} \int_0^T dt \int_{-\infty}^t dt' \frac{e^{i\epsilon'(t-t') + 2ik\omega t - 2ik'\omega t'}}{(t-t')^{3/2}} \times [e^{-iS'(t,t')} - \delta_{k,k'}], \quad (\text{A6})$$

$$S'(t, t') = \frac{1}{2} \int_{t'}^t P^2(\tau; t, t') d\tau, \quad (\text{A7})$$

$$\mathbf{P}(\tau; t, t') = \frac{1}{c} \left[\mathbf{A}'(\tau) - \frac{1}{t-t'} \int_{t'}^t \mathbf{A}'(\tau') d\tau' \right], \quad (\text{A8})$$

$$\mathcal{R}_0(E) = \sqrt{2E} [\cot \delta_0(E) - i], \quad (\text{A9})$$

where $\delta_0(E)$ is the s -wave scattering phase in the effective range approximation [24]. Since F_h is weak, the complex quasienergy ϵ' may be expressed as a sum of two terms: the complex quasienergy ϵ in the laser field described by vector potential $\mathbf{A}(t)$ and the linear in F_h correction, $\Delta\epsilon$, induced by the harmonic field described by the vector potential (A3),

$$\epsilon' = \epsilon + \Delta\epsilon.$$

Thus Eq. (A4) can be written in the equivalent form:

$$\mathbf{d}(N) = -2 \frac{\partial \Delta\epsilon}{\partial \mathbf{F}_h^*}. \quad (\text{A10})$$

Expanding the matrix elements $M'_{k,k'}(\epsilon')$ in a power series in F_h , one obtains an explicit expression for $\Delta\epsilon$:

$$\Delta\epsilon = -\frac{\kappa \mathcal{C}_0^2}{2} \sum_{k,k'} f_k [m_{k,k'}(\Omega_h) + m_{k,k'}(-\Omega_h)] f_{k'}, \quad (\text{A11})$$

where $f_k = f'_k|_{F_h=0}$, \mathcal{C}_0 is the dimensionless asymptotic coefficient of the atom's valence electron wave function [see Eq. (6)], and the matrix elements $m_{k,k'}(\pm\Omega_h) \propto F_h$ can be expressed in terms of two-dimensional time integrals. Specifically, the matrix elements $m_{k,k'}(\Omega_h)$ describe emission of a harmonic with frequency Ω_h and thus determine the HHG amplitude, while the matrix elements $m_{k,k'}(-\Omega_h)$ describe the absorption of a harmonic photon. In order to obtain perturbative results in F_Ω for the HHG amplitude, we further expand the matrix elements $m_{k,k'}(\Omega_h)$ in a power series in F_Ω :

$$m_{k,k'}(\Omega_h) \approx m_{k,k'}^{(0)}(\Omega_h) + m_{k,k'}^{(1)}(\Omega_h), \quad (\text{A12a})$$

$$m_{k,k'}^{(0)}(\Omega_h) = \frac{-i}{\sqrt{2\pi i}} \frac{1}{T} \int_0^T dt \int_{-\infty}^t dt' \frac{e^{-iS(t,t') + 2ik\omega t - 2ik'\omega t'}}{(t-t')^{3/2}} \times S_h^{(0)}(t, t'), \quad (\text{A12b})$$

$$m_{k,k'}^{(1)}(\Omega_h) = \frac{-i}{\sqrt{2\pi i}} \frac{1}{T} \int_0^T dt \int_{-\infty}^t dt' \frac{e^{-iS(t,t')} + 2ik\omega t - 2ik'\omega t'}{(t-t')^{3/2}} \times [S_h^{(1)}(t,t') - iS_h^{(0)}(t,t')S_\Omega(t,t')], \quad (\text{A12c})$$

where the functions $S_\Omega(t,t')$ and $S_h^{(n)}(t,t')$ originate from the first-order correction to the action $\mathcal{S}(t,t')$ in both the XUV and harmonic fields:

$$\mathcal{S}(t,t') = I_p(t-t') + \frac{1}{2} \int_{t'}^t P_0^2(\tau;t,t') d\tau, \quad (\text{A13a})$$

$$S_\Omega(t,t') = \int_{t'}^t P_0(\tau;t,t') P_1(\tau;t,t') d\tau, \quad (\text{A13b})$$

$$S_h^{(n)}(t,t') = \int_{t'}^t P_n(\tau;t,t') P_h(\tau;t,t') d\tau, \quad (\text{A13c})$$

$$\mathbf{P}_n(\tau;t,t') \equiv \mathbf{P}_n(\tau) = \frac{1}{c} \left[\mathbf{A}_n(\tau) - \frac{1}{t-t'} \int_{t'}^t \mathbf{A}_n(\tau') d\tau' \right], \quad n = 0, 1, \quad (\text{A13d})$$

$$\mathbf{P}_h(\tau;t,t') \equiv \mathbf{P}_h(\tau) = \frac{1}{c} \left[\mathbf{A}_h^{(+)}(\tau) - \frac{1}{t-t'} \int_{t'}^t \mathbf{A}_h^{(+)}(\tau') d\tau' \right], \quad (\text{A13e})$$

$$\mathbf{A}_h^{(+)}(t) = -c \frac{\mathbf{F}_h^*}{2i\Omega_h} e^{i\Omega_h t}. \quad (\text{A13f})$$

In Eqs. (A12) we have neglected the Stark shift and laser-induced width of the atomic level in the IR field.

It should be noticed that, for the two-component field (A2), the coefficients f_k should also be expanded in a power series in F_Ω . However, as was shown in Ref. [55], this correction to the coefficients f_k gives a negligible contribution to the total harmonic amplitude. Thus, in all further calculations we assume that the coefficients f_k originate from the IR field alone, i.e., $f_k \approx f_k^{(0)}$. The coefficients $f_k^{(0)}$ satisfy the eigenvalue system of equations (A5) with the substitution $\mathbf{A}^{\prime}(t) \rightarrow \mathbf{A}_0(t)$.

Both $S_\Omega(t,t')$ and $S_h^{(0)}(t,t')$ involve a product of a rapidly oscillating function, $P_1(\tau)$ or $P_h(\tau)$, and a smooth function, $P_0(\tau)$. Now, for a smooth function $\varphi(t)$ and a rapidly oscillating function $g(t)$, one can make the approximation,

$$\int_{t'}^t \varphi(\tau) g(\tau) d\tau \approx \varphi(t) G(t) - \varphi(t') G(t'), \quad G(t) = \int_{t'}^t g(\tau) d\tau. \quad (\text{A14})$$

Using the approximation (A14), the functions $S_\Omega^{(0)}(t,t')$, $S_h^{(0)}(t,t')$, and $S_h^{(1)}(t,t')$ can be presented in the form

$$S_h^{(0)}(t,t') = \frac{(\mathbf{F}_h^* \cdot \mathbf{e}_z)}{2\Omega_h^2} \chi_0(\Omega_h), \quad (\text{A15a})$$

$$S_\Omega^{(0)}(t,t') = \frac{F_\Omega}{2\Omega^2} [\chi_0(-\Omega) + \chi_0(\Omega)], \quad (\text{A15b})$$

$$\chi_0(\Omega) = P_0(t) e^{i\Omega t} - P_0(t') e^{i\Omega t'}, \quad (\text{A15c})$$

$$S_h^{(1)}(t,t') = \frac{(\mathbf{F}_h^* \cdot \mathbf{e}_z)}{4i\Omega_h \Omega} [\chi_1(-\Omega; \Omega_h) - \chi_1(\Omega; \Omega_h)], \quad (\text{A15d})$$

$$\chi_1(\Omega; \Omega_h) = \frac{e^{i(\Omega_h + \Omega)t} - e^{i(\Omega_h + \Omega)t'}}{\Omega_h + \Omega} + \frac{(e^{i\Omega_h t} - e^{i\Omega_h t'})(e^{i\Omega t} - e^{i\Omega t'})}{i\Omega_h \Omega (t-t')}. \quad (\text{A15e})$$

Substituting Eqs. (A15) into Eqs. (A12) and calculating the derivative in (A10), we obtain an explicit form for $\mathbf{d}(N)$:

$$\mathbf{d}(N) \approx \mathbf{d}^{(0)}(N) + \mathbf{d}^{(-1)}(N) + \mathbf{d}^{(+1)}(N), \quad (\text{A16})$$

$$\mathbf{d}^{(i)}(N) = \mathbf{e}_z \sum_{k,k'} f_k d_{k,k'}^{(i)}(N) f_{k'}, \quad i = 0, \pm 1,$$

where

$$d_{k,k'}^{(i)}(N) = \frac{1}{T} \int_0^T dt \int_{-\infty}^t dt' \frac{e^{2ik\omega t - 2ik'\omega t'}}{(t-t')^{3/2}} \times e^{-iS(t,t')} g_i(t,t'), \quad i = 0, \pm 1, \quad (\text{A17})$$

$$g_0(t,t) = -\kappa C_0^2 \sqrt{\frac{1}{2\pi i}} \frac{1}{\Omega_h^2} \chi_0(\Omega_h), \quad (\text{A18})$$

$$g_{\pm 1}(t,t') = \pm \kappa C_0^2 \sqrt{\frac{1}{2\pi i}} \frac{F_\Omega}{4\Omega_h \Omega} \times \left[\chi_1(\pm\Omega, \Omega_h) \pm \frac{i}{\Omega\Omega_h} \chi_0(\pm\Omega) \chi_0(\Omega_h) \right]. \quad (\text{A19})$$

The dipole $\mathbf{d}^{(0)}(N)$ describes HHG in the IR field, while $\mathbf{d}^{(+1)}(N)$ and $\mathbf{d}^{(-1)}(N)$ describe HHG in the IR field assisted by emission and absorption of an XUV photon, respectively. We thus focus our further analysis on the $\mathbf{d}^{(0)}(N)$ and $\mathbf{d}^{(-1)}(N)$ dipoles.

In the quasiclassical limit, $\mathbf{d}^{(0)}(N)$ can be presented in the factorized form [16,23,58,74]:

$$\mathbf{d}^{(0)}(N) = \mathbf{e}_z a(E_0) f_{\text{rec}}^{(0)}(E_0), \quad E_0 = \Omega_h - I_p, \quad (\text{A20})$$

where $a(E_0)$ is a universal laser-induced factor,

$$a(E_0) = \frac{C_0}{\sqrt{2\pi i}} \frac{1}{T} \int_0^T dt \int_{-\infty}^t dt' \frac{e^{i(E_0 + I_p)t - iS(t,t')}}{(t-t')^{3/2}}, \quad (\text{A21})$$

and $f_{\text{rec}}^{(0)}(E_0)$ is the TDER photorecombination amplitude for a model atomic system having a single bound s state [cf. Eq. (5)]:

$$f_{\text{rec}}^{(0)}(E_0) = -i\sqrt{\pi\kappa} C_0 \frac{k_0^2}{\Omega_h^2}, \quad k_0 = \sqrt{2E_0}. \quad (\text{A22})$$

In order to obtain a beyond-SFA result for the HHG amplitude with absorption of a single XUV photon, we use the first-order rescattering approximation, i.e., we present both coefficients f_k and matrix elements $d_{k,k'}^{(-1)}(N)$ as a sum of direct (with bar) and rescattering (with tilde) terms:

$$d_{k,k'}^{(-1)} \approx \overline{d_{k,k'}^{(-1)}} + \widetilde{d_{k,k'}^{(-1)}}, \quad f_k \approx \overline{f_k} + \widetilde{f_k}.$$

The direct and rescattering results for the coefficients f_k are [75,76]

$$\begin{aligned}\bar{f}_k &= \delta_{k,0}, \\ \tilde{f}_k &= \frac{M_{k,0}}{\mathcal{R}_0(-I_p + 2k\omega)},\end{aligned}$$

where the matrix element $M_{k,0} \equiv M_{k,0}(-I_p)$ can be obtained from $M'_{k,0}(\epsilon')$ by making the replacements $\mathbf{A}'(t) \rightarrow \mathbf{A}_0(t)$ and $\epsilon' \rightarrow -I_p$:

$$M_{k,0} = \frac{1}{\sqrt{2\pi i}} \frac{1}{T} \int_0^T dt \int_{-\infty}^t dt' \frac{e^{2ik\omega t - iS(t,t')}}{(t-t')^{3/2}}, \quad (\text{A23})$$

where $S(t, t')$ is given by Eq. (A13a).

The direct and rescattering terms for the matrix element $d_{k,k'}^{(-1)}(N)$ originate from different parts of the integral (A17). The direct term is given by the contribution of the boundary limit $t' \approx t$ to the integral (A17), while the rescattering term is given by the saddle-point contribution to the integral (A17). Up to the first-order rescattering approximation (defined above), the dipole moment $\mathbf{d}^{(-1)}(N)$ can be presented as follows:

$$\begin{aligned}\mathbf{d}^{(-1)}(N) &\approx \mathbf{e}_z d^{(-1)}(N), \\ d^{(-1)}(N) &= \sum_k \overline{d_{0,k}^{(-1)}}(N) \tilde{f}_k + \widetilde{d_{0,0}^{(-1)}}(N),\end{aligned} \quad (\text{A24})$$

where $\overline{d_{0,k}^{(-1)}}(N)$ is the matrix element for the “direct” dipole and $\widetilde{d_{0,0}^{(-1)}}(N)$ is that for the “rescattering” dipole. Analysis of the direct dipole matrix elements for a given harmonic number N shows that the matrix element $\overline{d_{0,k}^{(-1)}}(N)$ with $k = \bar{k} = (\Omega_h - \Omega)/(2\omega)$ exceeds all others by a factor of order $\sim (F/\kappa^3)^{-2}$. The leading term for this matrix element can be calculated analytically by evaluating the integral (A17) near the boundary limit $t' \approx t$:

$$\begin{aligned}\overline{d_{0,\bar{k}}^{(-1)}}(N) &= -\kappa \mathcal{C}_0 \frac{F\Omega}{4\Omega_h\Omega} \\ &\times \left[\frac{\kappa + ik_1}{\Omega_h - \Omega} + \frac{\kappa^3 + ik_1^3 - ik_\Omega^3 - ik_{\Omega_h}^3}{3\Omega\Omega_h} \right],\end{aligned} \quad (\text{A25})$$

where

$$\begin{aligned}\kappa &= \sqrt{2I_p}, \quad k_1 = \sqrt{2E_1}, \\ k_\Omega &= \sqrt{2(E_1 + \Omega)}, \quad k_{\Omega_h} = \sqrt{2(E_1 - \Omega_h)},\end{aligned} \quad (\text{A26})$$

and $E_1 = \Omega_h - I_p - \Omega$ is the returning electron energy. The explicit form (A25) for the direct term can be also found analytically as the value of $\overline{d_{0,k}^{(-1)}}(N)$ in the limit $F \rightarrow 0$ [23].

In order to evaluate the rescattering term $\widetilde{d_{0,0}^{(-1)}}(N)$ in (A24), we note that the function $g_{-1}(t, t')$ in Eq. (A19) involves four terms, which correspond to different scenarios for interaction of the electron with either the XUV or the harmonic field. In this paper, our focus is exclusively on the channels in which the electron absorbs one or more XUV photons and emits a harmonic at the recombination step of HHG, i.e., at the moment t . To separate out the channel

involving absorption of one XUV photon, we replace the functions χ_0 and χ_1 in (A15) by

$$\chi_0(-\Omega) \rightarrow P_0(t) e^{-i\Omega t}, \quad (\text{A27a})$$

$$\chi_0(\Omega_h) \rightarrow P_0(t) e^{i\Omega_h t}, \quad (\text{A27b})$$

$$\chi_1(-\Omega, \Omega_h) \rightarrow \frac{e^{i(\Omega_h - \Omega)t}}{\Omega_h - \Omega}. \quad (\text{A27c})$$

The approximations (A27) follow from Eqs. (A15c) and (A15e) by neglecting terms involving exponents dependent on the time t' and also the term $\sim (t-t')^{-1}$ in Eq. (A15e), since it is smaller than the term $\sim (t-t')^0$ by a factor of order ω/Ω . Taking into account the approximations (A27), the rescattering part of the dipole matrix element for the desired channel can be presented in the form

$$\begin{aligned}\widetilde{d_{0,0}^{(-1)}}(N) &= -\kappa \mathcal{C}_0 \sqrt{\frac{1}{2\pi i}} \frac{F\Omega}{4\Omega_h\Omega} \frac{1}{T} \\ &\times \int_0^T dt \int_{-\infty}^{t-0} dt' \frac{e^{-iS(t,t') + i(\Omega_h - \Omega)t}}{(t-t')^{3/2}} \\ &\times \left(\frac{1}{\Omega_h - \Omega} + \frac{P_0^2(t)}{\Omega_h\Omega} \right).\end{aligned} \quad (\text{A28})$$

The integrations in the rescattering terms for \tilde{f}_k in Eq. (A23) and for $\widetilde{d_{0,0}^{(-1)}}$ in Eq. (A28) are done using saddle-point methods [77]. In this approximation, the smooth function $P_0(t)$ can be replaced by its value at the corresponding saddle point, $P_0(t) \rightarrow k_1$, leading to the following result for the dipole matrix element $d^{(-1)}(N)$:

$$d^{(-1)}(N) = F\Omega a(E_1) f_{\text{rec}}^{(1)}(E_1). \quad (\text{A29})$$

The laser factor, $a(E_1)$, has the same form as for an IR field alone [see Eq. (A21)], and $f_{\text{rec}}^{(1)}(E_1)$ is the *exact* two-photon TDER recombination amplitude for absorption of an Ω photon and emission of an Ω_h photon [59]:

$$\begin{aligned}f_{\text{rec}}^{(1)}(E_1) &= -\frac{\sqrt{\pi\kappa}\mathcal{C}_0}{2\Omega\Omega_h} \left\{ \frac{k_1^2}{\Omega\Omega_h} + \frac{1}{\Omega_h - \Omega} \right. \\ &\left. + \frac{1}{\mathcal{R}_0(E_1)} \left[\frac{\kappa + ik_1}{\Omega_h - \Omega} + \frac{\kappa^3 + ik_1^3 - ik_\Omega^3 - ik_{\Omega_h}^3}{3\Omega\Omega_h} \right] \right\}.\end{aligned} \quad (\text{A30})$$

In Eq. (A30) the definitions in Eqs. (A26) and (13) have been used.

The laser factor, $a(E_n)$, takes its simplest analytical form in the energy region close to the cutoff of the HHG plateau. It is well known that only two closed classical electron trajectories with the highest returning energy contribute to the total HHG amplitude in this energy region. The calculations of the twofold integrals can be carried out by using a combination of saddle-point methods appropriate for separate and for merging saddle points. The explicit form of the laser factor can be expressed in terms of an Airy function $\text{Ai}(z)$ [16,58]:

$$a(E_n) = \frac{\tilde{\gamma} \sqrt{\Gamma_{\text{st}}(\tilde{F})} e^{i\Phi_0}}{\pi\kappa^{1/2} (\delta F)^{1/3} \Delta t^{3/2}} \text{Ai} \left[\frac{E_n - E_{\text{max}}}{(\delta F)^{1/3}} \right], \quad (\text{A31})$$

where $\Gamma_{\text{st}}(\tilde{F})$ is the detachment rate in a static electric field [see Eq. (18)], $\tilde{F} \approx 0.95F$ is the instantaneous electric field at the moment of ionization, $\tilde{\gamma} = \omega\kappa/\tilde{F}$ is an “effective” Keldysh parameter, $\Delta t \approx 0.65T$ is the electron travel time,

$E_{\text{max}} \approx 3.17u_p + 0.324I_p$ is the maximum energy gained, $\delta = 0.536$, and Φ_0 is the phase gained. Thus, in accordance with Eq. (14), one obtains the general form of the EWP given in Eqs. (16)–(19).

-
- [1] T. Popmintchev, M.-C. Chen, P. Arpin, M. M. Murnane, and H. C. Kapteyn, The attosecond nonlinear optics of bright coherent x-ray generation, *Nat. Photon.* **4**, 822 (2010).
- [2] T. Popmintchev, M.-C. Chen, D. Popmintchev, P. Arpin, S. Brown, S. Ališauskas, G. Andriukaitis, T. Balčiūnas, O. D. Mücke, A. Pugzlys, A. Baltuška, B. Shim, S. E. Schrauth, A. Gaeta, C. Hernández-García, L. Plaja, A. Becker, A. Jaron-Becker, M. M. Murnane, and H. C. Kapteyn, Bright coherent ultrahigh harmonics in the keV x-ray regime from mid-infrared femtosecond lasers, *Science* **336**, 1287 (2012).
- [3] D. Popmintchev, B. R. Galloway, M.-C. Chen, F. Dollar, C. A. Mancuso, A. Hankla, L. Miaja-Avila, G. O’Neil, J. M. Shaw, G. Fan, S. Ališauskas, G. Andriukaitis, T. Balčiūnas, O. D. Mücke, A. Pugzlys, A. Baltuška, H. C. Kapteyn, T. Popmintchev, and M. M. Murnane, Near- and Extended-Edge X-Ray-Absorption Fine-Structure Spectroscopy Using Ultrafast Coherent High-Order Harmonic Supercontinua, *Phys. Rev. Lett.* **120**, 093002 (2018).
- [4] P. Agostini and L. F. DiMauro, The physics of attosecond light pulses, *Rep. Prog. Phys.* **67**, 813 (2004).
- [5] P. B. Corkum and F. Krausz, Attosecond science, *Nat. Phys.* **3**, 381 (2007).
- [6] F. Krausz and M. Ivanov, Attosecond physics, *Rev. Mod. Phys.* **81**, 163 (2009).
- [7] *Attosecond Physics: Attosecond Measurements and Control of Physical Systems*, edited by L. Plaja, R. Torres, and A. Zaïr (Springer-Verlag, Berlin, 2013).
- [8] *Attosecond and xuv Physics: Ultrafast Dynamics and Spectroscopy*, edited by T. Schultz and M. Vrakking (Wiley-VCH, Weinheim, 2014).
- [9] M. Uiberacker, Th. Uphues, M. Schultze, A. J. Verhoef, V. Yakovlev, M. F. Kling, J. Rauschenberger, N. M. Kabachnik, H. Schröder, M. Lezius, K. L. Kompa, H. G. Muller, M. J. J. Vrakking, S. Hendel, U. Kleineberg, U. Heinzmann, M. Drescher, and F. Krausz, Attosecond real-time observation of electron tunnelling in atoms, *Nature (London)* **446**, 627 (2007).
- [10] L.-Y. Peng, W.-C. Jiang, J.-W. Geng, W.-H. Xiong, and Q. Gong, Tracing and controlling electronic dynamics in atoms and molecules by attosecond pulses, *Phys. Rep.* **575**, 1 (2015).
- [11] J. Itatani, J. Levesque, D. Zeidler, H. Niikura, H. Pépin, J. C. Kieffer, P. B. Corkum, and D. M. Villeneuve, Tomographic imaging of molecular orbitals, *Nature (London)* **432**, 867 (2004).
- [12] H. J. Wörner, H. Niikura, J. B. Bertrand, P. B. Corkum, and D. M. Villeneuve, Observation of Electronic Structure Minima in High-Harmonic Generation, *Phys. Rev. Lett.* **102**, 103901 (2009).
- [13] A. D. Shiner, B. E. Schmidt, C. Trallero-Herrero, H. J. Wörner, S. Patchkovskii, P. B. Corkum, J.-C. Kieffer, F. Légaré, and D. M. Villeneuve, Probing collective multi-electron dynamics in xenon with high-harmonic spectroscopy, *Nat. Phys.* **7**, 464 (2011).
- [14] T. Morishita, A.-T. Le, Z. Chen, and C. D. Lin, Accurate Retrieval of Structural Information from Laser-Induced Photoelectron and High-Order Harmonic Spectra by Few-Cycle Laser Pulses, *Phys. Rev. Lett.* **100**, 013903 (2008).
- [15] A.-T. Le, T. Morishita, and C. D. Lin, Extraction of the species-dependent dipole amplitude and phase from high-order harmonic spectra in rare-gas atoms, *Phys. Rev. A* **78**, 023814 (2008).
- [16] M. V. Frolov, N. L. Manakov, T. S. Sarantseva, M. Yu. Emelin, M. Yu. Ryabikin, and A. F. Starace, Analytic Description of the High-Energy Plateau in Harmonic Generation by Atoms: Can the Harmonic Power Increase with Increasing Laser Wavelengths? *Phys. Rev. Lett.* **102**, 243901 (2009).
- [17] A. D. Shiner, B. E. Schmidt, C. Trallero-Herrero, P. B. Corkum, J.-C. Kieffer, F. Légaré, and D. M. Villeneuve, Observation of Cooper minimum in krypton using high harmonic spectroscopy, *J. Phys. B* **45**, 074010 (2012).
- [18] M. C. H. Wong, A.-T. Le, A. F. Alharbi, A. E. Boguslavskiy, R. R. Lucchese, J.-P. Brichta, C. D. Lin, and V. R. Bhardwaj, High Harmonic Spectroscopy of the Cooper Minimum in Molecules, *Phys. Rev. Lett.* **110**, 033006 (2013).
- [19] M. V. Frolov, T. S. Sarantseva, N. L. Manakov, K. D. Fulfer, B. P. Wilson, J. Troß, X. Ren, E. D. Poliakoff, A. A. Silaev, N. V. Vvedenskii, A. F. Starace, and C. A. Trallero-Herrero, Atomic photoionization experiment by harmonic-generation spectroscopy, *Phys. Rev. A* **93**, 031403(R) (2016).
- [20] Y. Mairesse, J. Levesque, N. Dudovich, P. B. Corkum, and D. M. Villeneuve, High harmonic generation from aligned molecules—amplitude and polarization, *J. Mod. Opt.* **55**, 2591 (2008).
- [21] C. D. Lin, A.-T. Le, Z. Chen, T. Morishita, and R. Lucchese, Strong-field rescattering physics—self-imaging of a molecule by its own electrons, *J. Phys. B* **43**, 122001 (2010).
- [22] J. B. Bertrand, H. J. Wörner, P. Hockett, D. M. Villeneuve, and P. B. Corkum, Revealing the Cooper Minimum of N₂ by Molecular Frame High-Harmonic Spectroscopy, *Phys. Rev. Lett.* **109**, 143001 (2012).
- [23] M. V. Frolov, N. L. Manakov, T. S. Sarantseva, and A. F. Starace, Analytic confirmation that the factorized formula for harmonic generation involves the exact photorecombination cross section, *Phys. Rev. A* **83**, 043416 (2011).
- [24] L. D. Landau and E. M. Lifshitz, *Quantum Mechanics (Non-Relativistic Theory)*, 3rd ed. (Pergamon Press, Oxford, 1977).
- [25] I. I. Sobelman, *Atomic Spectra and Radiative Transitions* (Springer-Verlag, Berlin, 1979), Sec. 9.5.2.
- [26] V. B. Berestetskii, E. M. Lifshitz, and L. P. Pitaevskii, *Quantum Electrodynamics*, 2nd ed. (Pergamon, Oxford, 1982), Sec. 56.
- [27] P. B. Corkum, Plasma Perspective on Strong-Field Multiphoton Ionization, *Phys. Rev. Lett.* **71**, 1994 (1993).
- [28] A. Heinrich, W. Kornelis, M. P. Anscombe, C. P. Hauri, P. Schlup, J. Biegert, and U. Keller, Enhanced VUV-assisted high harmonic generation, *J. Phys. B* **39**, S275 (2006).

- [29] E. J. Takahashi, T. Kanai, K. L. Ishikawa, Y. Nabekawa, and K. Midorikawa, Dramatic Enhancement of High-Order Harmonic Generation, *Phys. Rev. Lett.* **99**, 053904 (2007).
- [30] F. Brizuela, C. M. Heyl, P. Rudawski, D. Kroon, L. Rading, J. M. Dahlström, J. Mauritsson, P. Johnsson, C. L. Arnold, and A. L'Huillier, Efficient high-order harmonic generation boosted by below-threshold harmonics, *Sci. Rep.* **3**, 1410 (2013).
- [31] M. Meyer, D. Cubaynes, P. O'Keeffe, H. Luna, P. Yeates, E. T. Kennedy, J. T. Costello, P. Orr, R. Taïeb, A. Maquet, S. Düsterer, P. Radcliffe, H. Redlin, A. Azima, E. Plönjes, and J. Feldhaus, Two-color photoionization in XUV free-electron and visible laser fields, *Phys. Rev. A* **74**, 011401(R) (2006).
- [32] K. Ishikawa, Photoemission and Ionization of He⁺ under Simultaneous Irradiation of Fundamental Laser and High-Order Harmonic Pulses, *Phys. Rev. Lett.* **91**, 043002 (2003).
- [33] K. L. Ishikawa, Efficient photoemission and ionization of He⁺ by a combined fundamental laser and high-order harmonic pulse, *Phys. Rev. A* **70**, 013412 (2004).
- [34] K. Schiessl, E. Persson, A. Scrinzi, and J. Burgdörfer, Enhancement of high-order harmonic generation by a two-color field: Influence of propagation effects, *Phys. Rev. A* **74**, 053412 (2006).
- [35] S. V. Popruzhenko, D. F. Zaretsky, and W. Becker, High-order harmonic generation by an intense infrared laser pulse in the presence of a weak UV pulse, *Phys. Rev. A* **81**, 063417 (2010).
- [36] K. J. Schafer, M. B. Gaarde, A. Heinrich, J. Biegert, and U. Keller, Strong Field Quantum Path Control Using Attosecond Pulse Trains, *Phys. Rev. Lett.* **92**, 023003 (2004).
- [37] M. B. Gaarde, K. J. Schafer, A. Heinrich, J. Biegert, and U. Keller, Large enhancement of macroscopic yield in attosecond pulse train-assisted harmonic generation, *Phys. Rev. A* **72**, 013411 (2005).
- [38] J. Biegert, A. Heinrich, C. P. Hauri, W. Kornelis, P. Schlup, M. P. Anscombe, M. B. Gaarde, K. J. Schafer, and U. Keller, Control of high-order harmonic emission using attosecond pulse trains, *J. Mod. Opt.* **53**, 87 (2006).
- [39] C. Figueira de Morisson Faria, P. Salières, P. Villain, and M. Lewenstein, Controlling high-order harmonic generation and above-threshold ionization with an attosecond-pulse train, *Phys. Rev. A* **74**, 053416 (2006).
- [40] G.-T. Zhang, J. Wu, C.-L. Xia, and X.-S. Liu, Enhanced high-order harmonics and an isolated short attosecond pulse generated by using a two-color laser and an extreme-ultraviolet attosecond pulse, *Phys. Rev. A* **80**, 055404 (2009).
- [41] M. R. Miller, C. Hernández-García, A. Jaroń-Becker, and A. Becker, Targeting multiple rescatterings through VUV-controlled high-order harmonic generation, *Phys. Rev. A* **90**, 053409 (2014).
- [42] A. Fleischer and N. Moiseyev, Amplification of high-order harmonics using weak perturbative high-frequency radiation, *Phys. Rev. A* **77**, 010102(R) (2008).
- [43] A. Fleischer, Generation of higher-order harmonics upon the addition of high-frequency XUV radiation to IR radiation: Generalization of the three-step model, *Phys. Rev. A* **78**, 053413 (2008).
- [44] M. Tudorovskaya and M. Lein, High-harmonic generation with combined infrared and extreme ultraviolet fields, *J. Mod. Opt.* **61**, 845 (2014).
- [45] J. Heslar, D. A. Telnov, and S.-I. Chu, Subcycle dynamics of high-order-harmonic generation of He atoms excited by attosecond pulses and driven by near-infrared laser fields: A self-interaction-free time-dependent density-functional-theory approach, *Phys. Rev. A* **89**, 052517 (2014).
- [46] J. Heslar, D. A. Telnov, and S.-I. Chu, Subcycle dynamics of high-harmonic generation in valence-shell and virtual states of Ar atoms: A self-interaction-free time-dependent density-functional-theory approach, *Phys. Rev. A* **91**, 023420 (2015).
- [47] C. Buth, F. He, J. Ullrich, C. H. Keitel, and K. Z. Hatsagortsyan, Attosecond pulses at kiloelectronvolt photon energies from high-order-harmonic generation with core electrons, *Phys. Rev. A* **88**, 033848 (2013).
- [48] A. C. Brown and H. W. van der Hart, Extreme-Ultraviolet-Initiated High-Order Harmonic Generation: Driving Inner-Valence Electrons Using Below-Threshold-Energy Extreme-Ultraviolet Light, *Phys. Rev. Lett.* **117**, 093201 (2016).
- [49] J.-A. You, J. M. Dahlström, and N. Rohringer, Attosecond dynamics of light-induced resonant hole transfer in high-order-harmonic generation, *Phys. Rev. A* **95**, 023409 (2017).
- [50] J. Leeuwenburgh, B. Cooper, V. Averbukh, J. P. Marangos, and M. Ivanov, High-Order Harmonic Generation Spectroscopy of Correlation-Driven Electron Hole Dynamics, *Phys. Rev. Lett.* **111**, 123002 (2013).
- [51] J. Leeuwenburgh, B. Cooper, V. Averbukh, J. P. Marangos, and M. Ivanov, Reconstruction of correlation-driven electron-hole dynamics by high-harmonic-generation spectroscopy, *Phys. Rev. A* **90**, 033426 (2014).
- [52] C. Buth, M. C. Kohler, J. Ullrich, and C. H. Keitel, High-order harmonic generation enhanced by XUV light, *Opt. Lett.* **36**, 3530 (2011).
- [53] N. B. Delone, N. L. Manakov, and A. G. Fainshtein, Ionization of atoms by a low-frequency field and optical-frequency field, *Zh. Eksp. Teor. Fiz.* **86**, 906 (1984) [*Sov. Phys. JETP* **59**, 529 (1984)].
- [54] M. Lewenstein, Ph. Balcou, M. Yu. Ivanov, A. L'Huillier, and P. B. Corkum, Theory of high-harmonic generation by low-frequency laser fields, *Phys. Rev. A* **49**, 2117 (1994).
- [55] T. S. Sarantseva, M. V. Frolov, and N. V. Vvedenskii, Modification of the spectrum of high harmonics by a weak vacuum ultraviolet field, *Quantum Electron.* **48**, 625 (2018).
- [56] M. V. Frolov, N. L. Manakov, E. A. Pronin, and A. F. Starace, Model-Independent Quantum Approach for Intense Laser Detachment of a Weakly Bound Electron, *Phys. Rev. Lett.* **91**, 053003 (2003).
- [57] M. V. Frolov, N. L. Manakov, and A. F. Starace, Effective-range theory for an electron in a short-range potential and a laser field, *Phys. Rev. A* **78**, 063418 (2008).
- [58] M. V. Frolov, N. L. Manakov, T. S. Sarantseva, and A. F. Starace, Analytic formulae for high harmonic generation, *J. Phys. B* **42**, 035601 (2009).
- [59] A. N. Zheltukhin, N. L. Manakov, A. V. Flegel, and M. V. Frolov, Effects of the atomic structure and interference oscillations in the electron photorecombination spectrum in a strong laser field, *Zh. Eksp. Teor. Fiz. Pis'ma* **94**, 641 (2011) [*JETP Lett.* **94**, 599 (2011)].
- [60] O. Raz, O. Pedatzur, B. D. Bruner, and N. Dudovich, Spectral caustics in attosecond science, *Nat. Photon.* **6**, 170 (2012).
- [61] D. Faccialà, S. Pabst, B. D. Bruner, A. G. Ciriolo, S. De Silvestri, M. Devetta, M. Negro, H. Soifer, S. Stagira, N. Dudovich, and C. Vozzi, Probe of Multielectron Dynamics in

- Xenon by Caustics in High-Order Harmonic Generation, *Phys. Rev. Lett.* **117**, 093902 (2016).
- [62] D. Faccialà, S. Pabst, B. D. Bruner, A. G. Ciriolo, M. Devetta, M. Negro, P. Prasanna Geetha, A. Pusala, H. Soifer, N. Dudovich, S. Stagira, and C. Vozzi, High-order harmonic generation spectroscopy by recolliding electron caustics, *J. Phys. B* **51**, 134002 (2018).
- [63] B. M. Smirnov and M. I. Chibisov, The breaking up of atomic particles by an electric field and by electron collisions, *Zh. Eksp. Teor. Fiz.* **49**, 841 (1965) [*Sov. Phys. JETP* **22**, 585 (1966)].
- [64] M. V. Frolov, N. L. Manakov, A. A. Minina, S. V. Popruzhenko, and A. F. Starace, Adiabatic-limit Coulomb factors for photoelectron and high-order-harmonic spectra, *Phys. Rev. A* **96**, 023406 (2017).
- [65] V. S. Popov, Tunnel and multiphoton ionization of atoms and ions in a strong laser field (Keldysh theory), *Usp. Fiz. Nauk* **174**, 921 (2004) [*Phys.-Usp.* **47**, 855 (2004)].
- [66] S. V. Popruzhenko, Keldysh theory of strong field ionization: History, applications, difficulties and perspectives, *J. Phys. B* **47**, 204001 (2014).
- [67] A. A. Silaev, A. A. Romanov, and N. V. Vvedenskii, Multi-hump potentials for efficient wave absorption in the numerical solution of the time-dependent Schrödinger equation, *J. Phys. B* **51**, 065005 (2018).
- [68] A. F. Starace, Theory of atomic photoionization, in *Handbuch Der Physik*, edited by W. Mehlhorn (Springer-Verlag, Berlin, 1982), Vol. 31, pp. 1–121.
- [69] M. Ya. Amusia, *Atomic Photoeffect* (Springer, New York, 1990).
- [70] E. Ferrari, C. Spezzani, F. Fortuna, R. Delaunay, F. Vidal, I. Nikolov, P. Cinquegrana, B. Diviacco, D. Gauthier, G. Penco, P. R. Ribič, E. Roussel, M. Trovò, J.-B. Moussy, T. Pincelli, L. Lounis, M. Manfredda, E. Pedersoli, F. Capotondi, C. Svetina, N. Mahne, M. Zangrando, L. Raimondi, A. Demidovich, L. Giannessi, G. De Ninno, M. B. Danailov, E. Allaria, and M. Sacchi, Widely tunable two-colour seeded free-electron laser source for resonant-pump resonant-probe magnetic scattering, *Nat. Commun.* **7**, 10343 (2016).
- [71] Z. Zhao, H. Li, and Q. Jia, Generation of coherent two-color pulses at two adjacent harmonics in a seeded free-electron laser, *Phys. Rev. Accel. Beams* **21**, 020701 (2018).
- [72] L. Giannessi, E. Allaria, K. C. Prince, C. Callegari, G. Sansone, K. Ueda, T. Morishita, C. N. Liu, A. N. Grum-Grzhimailo, E. V. Gryzlova, N. Douguet, and K. Bartschat, Coherent control schemes for the photoionization of neon and helium in the extreme ultraviolet spectral region, *Sci. Rep.* **8**, 7774 (2018).
- [73] M. V. Frolov, A. V. Flegel, N. L. Manakov, and A. F. Starace, Description of harmonic generation in terms of the complex quasienergy. I. General formulation, *Phys. Rev. A* **75**, 063407 (2007).
- [74] M. V. Frolov, N. L. Manakov, A. M. Popov, O. V. Tikhonova, E. A. Volkova, A. A. Silaev, N. V. Vvedenskii, and A. F. Starace, Analytic theory of high-order-harmonic generation by an intense few-cycle laser pulse, *Phys. Rev. A* **85**, 033416 (2012).
- [75] M. V. Frolov, A. A. Khuskivadze, N. L. Manakov, and A. F. Starace, An analytical quantum model for intense field processes: Quantum origin of rescattering plateaus, *J. Phys. B* **39**, S283 (2006).
- [76] M. V. Frolov, D. V. Knyazeva, N. L. Manakov, J.-W. Geng, L.-Y. Peng, and A. F. Starace, Analytic model for the description of above-threshold ionization by an intense short laser pulse, *Phys. Rev. A* **89**, 063419 (2014).
- [77] R. Wong, *Asymptotic Approximations of Integrals* (SIAM, Philadelphia, 2001).